Plasma Sources Science and Technology

PAPER • **OPEN ACCESS**

Self-consistent electron–THF cross sections derived using data-driven swarm analysis with a neural network model

To cite this article: P W Stokes *et al* 2020 *Plasma Sources Sci. Technol.* **29** 105008

View the article online for updates and enhancements.

Recent citations

- Electron impact ionization of R-carvone: III. Absolute total ionization cross sections
R.A.A. Amorim *et al*

- An improved set of electron-THFA cross sections refined through a neural network-based analysis of swarm data
P. W. Stokes *et al*

IOP ebooks™

Bringing together innovative digital publishing with leading authors from the global scientific community.

Start exploring the collection–download the first chapter of every title for free.

This content was downloaded from IP address 137.219.201.94 on 12/04/2021 at 00:37

OPEN ACCESS
IOP Publishing

Plasma Sources Science and Technology

Plasma Sources Sci. Technol. **29** (2020) 105008 (10pp)

https://doi.org/10.1088/1361-6595/abb4f6

Self-consistent electron–THF cross sections derived using data-driven swarm analysis with a neural network model

P W Stokes[1,*], M J E Casey[1], D G Cocks[2], J de Urquijo[3], G García[4], M J Brunger[5,6] and R D White[1]

[1] College of Science and Engineering, James Cook University, Townsville, QLD 4811, Australia
[2] Research School of Physics, Australian National University, Canberra, ACT 0200, Australia
[3] Instituto de Ciencias Físicas, Universidad Nacional Autónoma de México, 62251, Cuernavaca, Morelos, Mexico
[4] Instituto de Física Fundamental, CSIC, Serrano 113-bis, 28006 Madrid, Spain
[5] College of Science and Engineering, Flinders University, Bedford Park, Adelaide, SA 5042, Australia
[6] Department of Actuarial Science and Applied Statistics, Faculty of Business and Management, UCSI University, Kuala Lumpur 56000, Malaysia

E-mail: peter.stokes@my.jcu.edu.au

Received 5 July 2020, revised 21 August 2020
Accepted for publication 3 September 2020
Published 16 October 2020

Abstract

We present a set of self-consistent cross sections for electron transport in gaseous tetrahydrofuran (THF), that refines the set published in our previous study [1] by proposing modifications to the quasielastic momentum transfer, neutral dissociation, ionisation and electron attachment cross sections. These adjustments are made through the analysis of pulsed-Townsend swarm transport coefficients, for electron transport in pure THF and in mixtures of THF with argon. To automate this analysis, we employ a neural network model that is trained to solve this inverse swarm problem for realistic cross sections from the LXCat project. The accuracy, completeness and self-consistency of the proposed refined THF cross section set is assessed by comparing the analyzed swarm transport coefficient measurements to those simulated via the numerical solution of Boltzmann's equation.

Keywords: swarm analysis, machine learning, artificial neural network, biomolecule

(Some figures may appear in colour only in the online journal)

1. Introduction

Accurate modeling of electron transport through human tissue is essential for a number of medical applications, including for treatment planning in medical physics, and for the control and optimisation of low-temperature atmospheric-pressure plasmas in plasma medicine [2–7]. To accurately simulate electron transport in biological media, a precise description of the energy deposition and electron loss/production from scattering with each constituent biomolecule is necessary. This description, which takes the form of electron impact cross sections [8], is required over a wide range of energies, as even subionising electrons are capable of damaging DNA through the process of dissociative electron attachment (DEA) [9–11].

One of the most well-studied biomolecules, after water, is tetrahydrofuran (THF, C_4H_8O), a simple surrogate for the complex sugar linking phosphate groups in the backbone of DNA [12, 13]. As such, numerous electron scattering cross sections have been measured and derived for THF. These include both experimental and theoretical derivations of the total [13–17], quasielastic [16, 18–23], vibrational excitation [20, 24–27], discrete electronic-state excitation [27, 28], ionisation [13, 29–34], and DEA cross sections [35, 36]. In total, six full sets of THF cross sections have been constructed.

* Author to whom any correspondence should be addressed.

 © 2020 The Author(s). Published by IOP Publishing Ltd Printed in the UK

This is an open access article distributed under the terms of the Creative Commons Attribution 4.0 License.
Any further distribution of this work must maintain attribution to the author(s) and the title of the work, journal citation and DOI.

Chronologically, these are due to Garland *et al* [37], for incident electron energies from 0.1 eV to 300 eV, Fuss *et al* [17], for energies from 1 eV to 10 keV, Bug *et al* [13], for energies from 30 eV to 1 keV, Swadia *et al* [34,38], for energies from the ionisation threshold to 5 keV, and Casey *et al* [39] who refined the Garland *et al* set by performing and analysing the first experimental measurements of swarm transport coefficients in pure THF. Subsequently, de Urquijo *et al* [1] further refined the Casey *et al* set by including transport coefficients for admixtures of THF in argon and nitrogen in the analysis. In the latter two studies, the *inverse swarm problem* of unfolding cross sections from swarm data was solved iteratively through the repeated adjustment of the cross section set until a good agreement was found between the simulated transport coefficients and experiment.

Swarm experiments provide a useful way to assess the accuracy and self-consistency of cross sections [40]. The iterative approach described above for analysing swarm data dates back to Mayer [41], Ramsauer [42] and Townsend and Bailey [43], who simulated swarm transport coefficients for comparison with experiment using approximate forms of the electron energy distribution function (EEDF). Since then swarm analysis has increased in sophistication, in particular since Phelps and collaborators [44–48] began determining the EEDF accurately through the numerical solution of Boltzmann's equation. Despite such improvements, it is important to note that, as an inverse problem, swarm analysis can become ill-posed when the amount of available experimental data is limited. That is, multiple underlying cross section sets can potentially result in the same collection of swarm transport coefficients. The success of iterative swarm analysis is thus often predicated on an expert performing the cross section adjustments, relying on their experience and intuition in order to avoid solutions that are unphysical. This holds true even for automated methods for swarm analysis via the numerical optimisation of transport coefficients [49–56] which, due to the ill-posed nature of the inverse swarm problem, can potentially become stuck in unphysical local minima that require the subsequent intervention and appraisal of an expert. In our recent work [57], we attempted to automate this expertise by training an artificial neural network model on cross sections derived from the LXCat project [58–60]. This neural network was applied quite successfully towards simultaneously deriving multiple cross sections of helium from simulated swarm data, showing the promise of this machine learning approach.

In this investigation, we apply the aforementioned data-driven swarm analysis in order to try and determine plausible improvements to the set of THF cross sections constructed by de Urquijo *et al* [1]. We begin in section 2 by outlining a suitable neural network for electron–THF swarm analysis, as well as an appropriate training procedure and a suitable set of training data. In section 3, we apply this neural network in order to analyze pulsed-Townsend drift velocities and Townsend first ionisation coefficients of electron transport in both pure THF and mixtures of THF in argon. As output from the network, we obtain for THF a quasielastic momentum transfer cross section (MTCS), a pair of neutral dissociation cross sections, an ionisation cross section, and an electron attachment cross section. With these machine-fitted cross sections in place of their counterparts in the de Urquijo *et al* set, we subsequently simulate pulsed-Townsend transport coefficients in section 4 to confirm that they coincide with the experimental measurements that were used as input to the neural network. Finally, we present conclusions in section 5 while also discussing avenues for future work.

2. Neural network for electron–THF swarm analysis

In this section, we provide a brief overview of the architecture and training of our neural network for the regression of THF cross sections given relevant sets of electron swarm transport coefficients. A more detailed introduction to this machine-assisted approach to swarm analysis can be found in our previous work [57].

2.1. Architecture

To obtain a solution to the inverse swarm problem for electron transport in THF, we apply a fully-connected neural network in order to determine the quasielastic (elastic + rotational) MTCS, $\sigma_\mathrm{m}(\varepsilon)$, the pair of neutral dissociation cross sections, $\sigma_{\mathrm{ex},1}(\varepsilon)$ and $\sigma_{\mathrm{ex},2}(\varepsilon)$, the ionisation cross section, $\sigma_\mathrm{io}(\varepsilon)$, and the electron attachment cross section, $\sigma_\mathrm{at}(\varepsilon)$, as illustrated by figure 1. The remaining excitation cross sections (e.g. for vibrational excitation and discrete electronic-state excitation) are not included here, as they are considered to be better known [1], and are instead sourced from the cross section set constructed by de Urquijo *et al* [1]. The neural network performs a nonlinear mapping from an input vector $\mathbf{x}$ containing swarm data, to an output vector $\mathbf{y}$ containing the aforementioned cross sections:

$$\mathbf{y} = \begin{bmatrix} \sigma_\mathrm{m}(\varepsilon) \\ \sigma_{\mathrm{ex},1}(\varepsilon) \\ \sigma_{\mathrm{ex},2}(\varepsilon) \\ \sigma_\mathrm{io}(\varepsilon) \\ \sigma_\mathrm{at}(\varepsilon) \end{bmatrix}. \tag{1}$$

As each output cross section is a function of energy, ε, this energy is made an input to the neural network, alongside the swarm transport coefficients:

$$\mathbf{x} = \begin{bmatrix} \varepsilon \\ W_1 \\ W_2 \\ \vdots \\ \left(\alpha_\mathrm{eff}/n_0\right)_1 \\ \left(\alpha_\mathrm{eff}/n_0\right)_2 \\ \vdots \end{bmatrix}, \tag{2}$$

where W denotes the flux drift velocity, α_eff/n_0 denotes the reduced effective Townsend first ionisation coefficient, and n_0 is the background neutral number density. Subscripts indicate that a number of pulsed-Townsend swarm measurements are

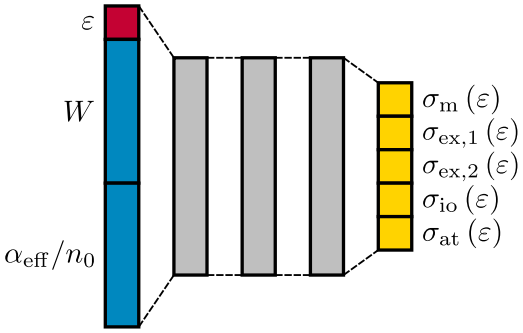

Figure 1. Diagram of the fully-connected neural network, equation (3), used for the regression of selected THF cross sections (yellow) as a function of energy (red) given some relevant electron swarm data (blue). Specifically, as output, the neural network provides the quasielastic MTCS, $\sigma_{\text{m}}(\varepsilon)$, the neutral dissociation cross sections, $\sigma_{\text{ex},1}(\varepsilon)$ and $\sigma_{\text{ex},2}(\varepsilon)$, the ionisation cross section $\sigma_{\text{io}}(\varepsilon)$, and the electron attachment cross section, $\sigma_{\text{at}}(\varepsilon)$. As input, in addition to the energy ε, the network takes drift velocities, W, and effective Townsend first ionisation coefficients, α_{eff}/n_0, both of which are measured for a variety of reduced electric fields, E/n_0, and admixture ratios of THF in argon. Cross section training data is chosen carefully, as described in section 2.2, so as to constrain the derived cross sections to be within the vicinity of their known uncertainties.

provided as input to the network. Mathematically, the neural network takes the form of the following composition of functions:

$$\mathbf{y}(\mathbf{x}) = (\mathbf{A}_4 \circ \text{swish} \circ \mathbf{A}_3 \circ \text{swish} \circ \mathbf{A}_2 \circ \text{swish} \circ \mathbf{A}_1)(\mathbf{x}), \tag{3}$$

where the $\text{swish}(x) \equiv x/\left(1+\text{e}^{-x}\right)$ nonlinear *activation function* [61] is applied element-wise throughout, and each $\mathbf{A}_n(\mathbf{x}) \equiv \mathbf{W}_n\mathbf{x} + \mathbf{b}_n$ is an affine transformation defined by a parameter matrix $\mathbf{W}_n$ and vector $\mathbf{b}_n$. It is these parameters that are optimised when training the neural network, as described in section 2.4 below. Note that the vectors $\mathbf{b}_1$, $\mathbf{b}_2$ and $\mathbf{b}_3$ are each made to contain 256 parameters, while $\mathbf{b}_4$ must contain 5 parameters, corresponding to the number of output cross sections. The matrices $\mathbf{W}_n$ are sized accordingly.

Finally, it is important to note that in what follows, the cross sections, energies, and transport coefficients are all log-transformed before being used to train the network, so as to ensure all training data lies within the domain $[-1, 1]$:

$$z \mapsto \log_{\sqrt{\frac{z_{\max}}{z_{\min}}}}\left(\frac{z}{\sqrt{z_{\max}z_{\min}}}\right), \tag{4}$$

where $z_{\min}$ and $z_{\max}$ are the extrema of all values of the quantity z employed for training. As this transformation is undefined when z is a cross section equal to zero, we replace such instances with a suitably small positive number, which we take to be $10^{-26}\,\text{m}^2$. In turn, if the neural network outputs a cross section less than $10^{-26}\,\text{m}^2$, we treat that output as being equal to zero instead. Threshold energies for the processes of neutral dissociation and ionisation can thus be inferred directly from the output of the neural network.

2.2. Cross section training data

We construct exemplar cross sections for training the neural network, equation (3), through the pairwise geometric combination of cross sections from the LXCat project [58–60, 64–81]. That is, given a random pair of LXCat cross sections, $\sigma_1(\varepsilon)$ and $\sigma_2(\varepsilon)$, of a given type (e.g. electron attachment, ionisation, etc), as well as a uniformly sampled mixing ratio $r \in [0, 1]$, a physically-plausible cross section of the same type is formed as:

$$\sigma(\varepsilon) = \sigma_1^{1-r}\left(\varepsilon+\varepsilon_1-\varepsilon_1^{1-r}\varepsilon_2^{r}\right)\sigma_2^{r}\left(\varepsilon+\varepsilon_2-\varepsilon_1^{1-r}\varepsilon_2^{r}\right), \tag{5}$$

where ε_1 and ε_2 are the respective threshold energies of $\sigma_1(\varepsilon)$ and $\sigma_2(\varepsilon)$. This formula has the benefit of retaining the correlation between the magnitude of a cross section and its threshold energy [57].

We apply equation (5) directly to generate suitable training examples for the electron attachment cross section, $\sigma_{\text{at}}(\varepsilon)$, and the lower-threshold neutral dissociation cross section, $\sigma_{\text{ex},1}(\varepsilon)$. No explicit constraints are placed on these cross sections, as seen by the large confidence bands for the training examples in figures 2(a) and (b). To emphasise this point, although we refer to $\sigma_{\text{ex},1}(\varepsilon)$ as the neutral dissociation cross section of 'lower threshold', some of its training examples have threshold energies that exceed that of the 'higher threshold' neutral dissociation cross section, $\sigma_{\text{ex},2}(\varepsilon)$.

For the remaining cross sections of interest, we choose to explicitly constrain the training cross sections to lie within the vicinity of the known experimental error bars so as to encourage the neural network to also restrict its output in the same way. To do this, in each case we apply equation (5) to first generate an unconstrained cross section by mixing the relevant LXCat cross sections, and then we apply equation (5) once more to mix this unconstrained cross section with its counterpart from the de Urquijo *et al* [1] set, weighting heavily towards the latter with a mixing ratio of $r = 0.9$. In this way our training cross sections are thus energy-dependent perturbations of the respective de Urquijo *et al* cross sections. The resulting confidence bands of these training examples can be seen plotted in figures 2(c)–(e).

Once the separate training cross sections are generated as described above, each are used to replace their counterpart in the de Urquijo *et al* set in order to obtain a proposed full data set of cross sections for training. Rejection sampling is then used to only keep generated cross section sets that have a grand total cross section (TCS) that lies within 30% of that of Fuss *et al* [17] and Fuss *et al* [62]. This constraint is illustrated by the confidence band in figure 2(f). In total, 5×10^4 such cross section sets are generated for use in the training procedure.

Note that, when training the neural network, cross sections must be sampled at discrete points within the energy domain, which we choose to be $\varepsilon \in \left[10^{-4}\text{ eV}, 10^{3}\text{ eV}\right]$. We select such points using:

$$\varepsilon = 10^{s}\text{ eV}, \tag{6}$$

where $s \in [-4, 3]$ is a uniformly distributed random number.

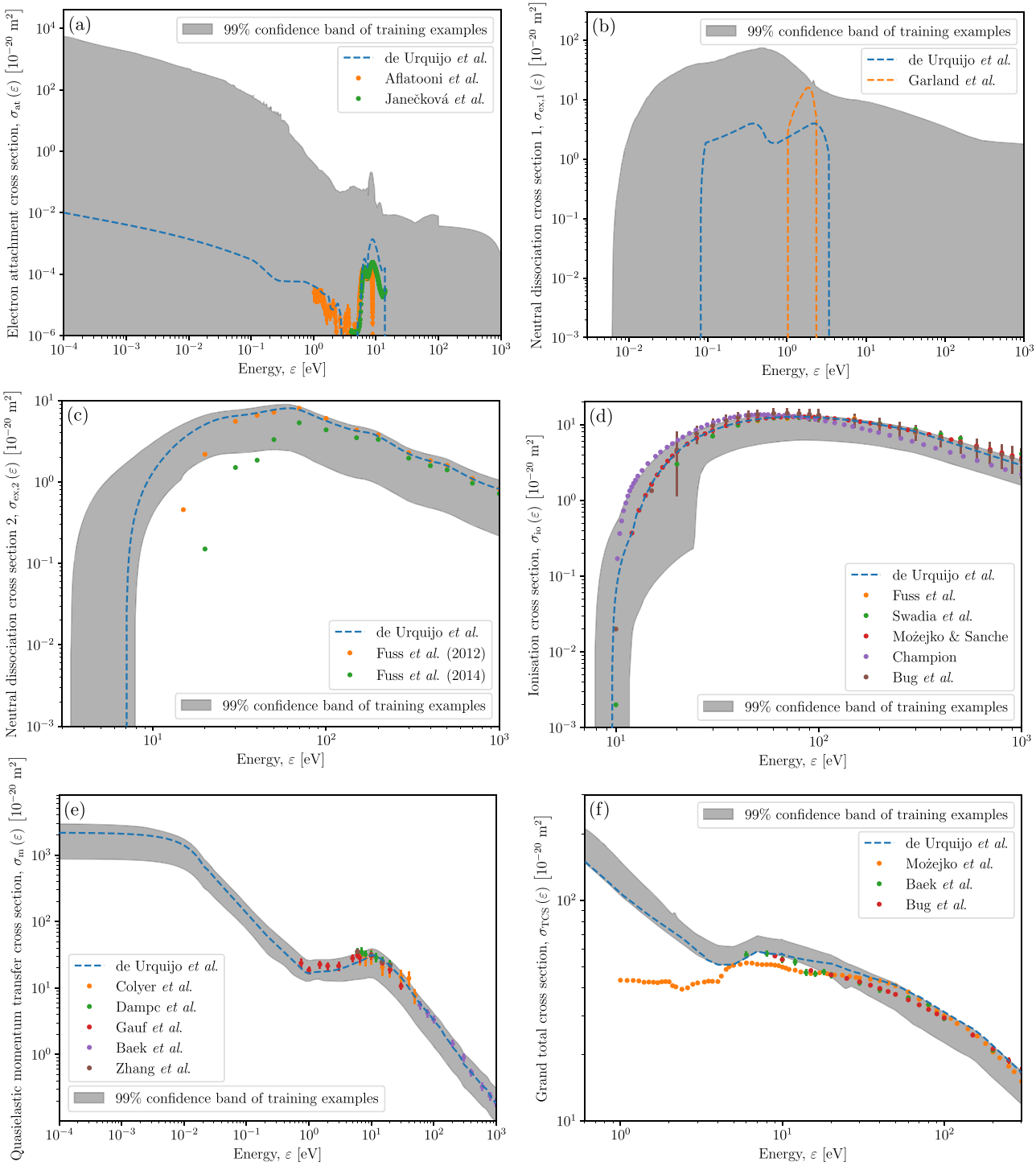

Figure 2. Confidence bands (grey) for exemplar cross sections used to train the neural network, equation (3). These training cross sections are derived from the LXCat project [58–60] using equation (5) and detailed in section 2.2. Through this choice of training data, the neural network is encouraged to derive a cross section set that is consistent with experimental and theoretical results from earlier studies [1,13,16–19,22,23,29,32,34–37,62,63], including those from the recent set of de Urquijo *et al* [1] (blue dashed lines).

2.3. Transport coefficient training data

Finally, to complete each input/output training pair, corresponding pulsed-Townsend swarm transport coefficients must be simulated. For this, we apply the two-term approximation [82, 83] to Boltzmann's equation and then perform backward prolongation [84] of the EEDF by inward integration from high to low energies, using an adaptive order adaptive energy Adams–Moulton method [85], as implemented in the *differentialequations.jl* software ecosystem [86–88].

As input to the neural network, we use drift velocities and reduced effective Townsend first ionisation coefficients measured using the pulsed-Townsend technique by de Urquijo *et al* [1] for electron transport in both pure THF,

as well as in admixtures of THF in argon. Specifically, these measurements were taken for THF mixture ratios of 1%, 2%, 5%, 10%, 20%, 50% and 100%, across a variety of reduced electric fields, E/n_0, ranging from 0.23 Td to 1000 Td, where 1 Td = 1 Townsend = 10^{-21} V m^2. For calculating the admixture transport coefficients, we use the argon cross section set present in the Biagi v7.1 database [65].

To account for the random error present in experimental measurements, we augment the aforementioned simulated transport coefficients by multiplying with a small amount of random noise before training sampled from a log-normal distribution. To be specific, we sample the natural logarithm of this noise factor from a normal distribution with a mean of 0 and a standard deviation of 0.01.

It should be noted that we have recently come to the view that as the experimental effective Townsend first ionisation coefficients below 10^{-24} m^2 are at the limit of the apparatus measurement capability, they should not be included in the present analysis and nor should they have been considered in the analysis of de Urquijo *et al* [1]. Because of this, as well as discrepancies attributed to Penning ionisation [1], we choose to exclude all 1% and 2% THF admixture effective Townsend first ionisation coefficients from our analysis.

2.4. Training procedure

We implement the neural network, equation (3), using the *Flux.jl* machine learning framework [89]. We initialise the neural network parameters in $\mathbf{b}_n$ to zero and those in $\mathbf{W}_n$ to uniform random numbers as described by Glorot and Bengio [90]. Then, we use the Adam optimiser [91], with step size $\alpha = 10^{-3}$, exponential decay rates $\beta_1 = 0.9$ and $\beta_2 = 0.999$, and small parameter $\epsilon = 10^{-8}$, to adjust the parameters so as to minimise the mean absolute error of the cross sections fitted by the neural network:

$$\frac{1}{5N}\sum_{i=1}^{N} \|\mathbf{y}_i - \boldsymbol{\sigma}\left(\mathbf{x}_i\right)\|_1, \tag{7}$$

where the index i ranges over the entire set of N training examples $\left(\mathbf{x}_i, \mathbf{y}_i\right)$, and $\boldsymbol{\sigma}\left(\mathbf{x}_i\right)$ is the associated neural network cross section prediction. We choose to optimise the mean absolute error, instead of the mean squared error, due to its robustness in the presence of outliers in the training data, which are expected in the parts of the underlying cross sections that are most uncertain. Specifically, the neural network parameters are updated by the optimiser repeatedly using batches of 4096 input/output training examples, each consisting of 16 random LXCat-derived cross section sets selected from the 5×10^4 generated in total, where each set is sampled with equation (6) at 256 random energies within the domain $\left[10^{-4}\text{ eV}, 10^3\text{ eV}\right]$. Training is continued until the transport coefficients, resulting from the fitted cross section set, best match the pulsed-Townsend transport coefficients that were used to perform the fit.

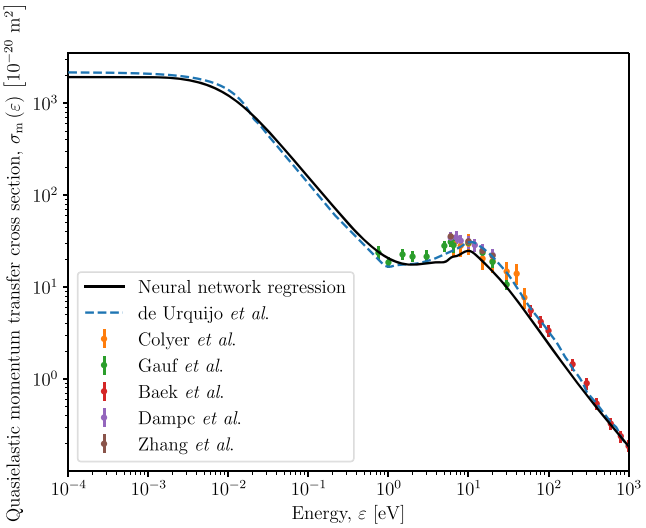

Figure 3. Previous quasielastic MTCSs [1, 16, 18, 19, 22, 23], compared to that determined from our neural network regression approach.

3. Machine-fitted THF cross sections

In this section, we present the resulting electron–THF cross sections that were determined automatically from swarm data by using the neural network, equation (3), described in the previous section. It should be noted that, when these cross sections are used to simulate/reproduce the aforementioned swarm data, the resulting mean electron energies for the swarms vary between 0.03 eV and 7.77 eV. As such, cross sections that are significantly outside of this energy range are unlikely to have a large effect on the considered swarm transport coefficients. In these regimes of very small or very large energies, it is thus expected that the neural network would rely more heavily on its prior knowledge of what constitutes a physically-plausible cross section than on the swarm measurements themselves.

3.1. Quasielastic MTCS

Overall, the machine-fitted quasielastic MTCS does not deviate far from that of de Urquijo *et al* [1], as shown in figure 3, and as such agrees reasonably well with the experimental and calculated cross sections of Coyler *et al* [18], Gauf *et al* [22], Baek *et al* [16], Dampc *et al* [19], and Zhang *et al* [23]. At very low energies, below 10^{-2} eV, the neural network predicts a roughly constant quasielastic MTCS that is about 10% smaller in magnitude compared to that of the de Urquijo *et al* counterpart in the same energy regime. The greatest relative deviation from the de Urquijo *et al* cross section occurs around 25 eV, where the cross section determined by the neural network is smaller by 30%.

3.2. Neutral dissociation cross section

The low-threshold energy neutral dissociation cross section found by the neural network highlights the non-uniqueness of this inverse swarm problem, as it differs substantially from that of both Garland *et al* [37] and de Urquijo *et al* [1], as seen in figure 4(a). To begin with, the fitted threshold energy is equal

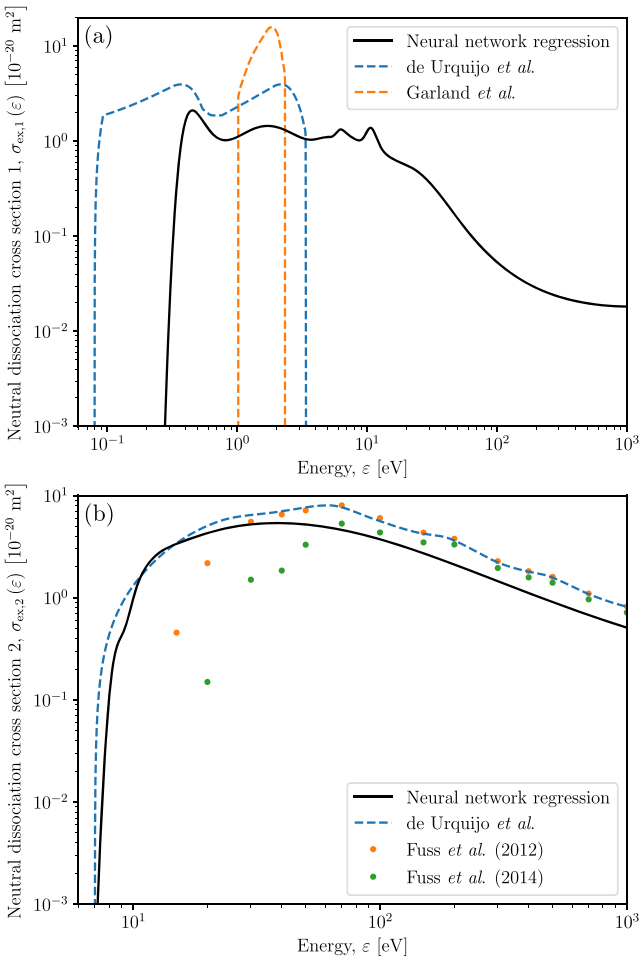

Figure 4. A comparison of the low and high energy neutral dissociation cross sections, (a) and (b), as determined from the present neural network regression and from previous studies [1, 17, 37, 62].

to 0.23 eV, lying between the thresholds of 0.08 eV for de Urquijo *et al* and 1eV for Garland *et al*. Additionally, the cross section magnitude is also smaller than both aforementioned counterparts, with a peak of 2×10^{-20} m^2. From its maximum value, this neutral dissociation cross section remains roughly constant until 10 eV, where it decays by roughly two orders of magnitude by 1000 eV.

The fitted high-threshold energy neutral dissociation cross section, plotted in figure 4(b), can be seen to have a smaller threshold energy of 6.3 eV compared to the 7 eV used by de Urquijo *et al*. In general, this cross section prediction lies below its de Urquijo *et al* counterpart, by up to 40% at high energies. This puts this machine-fitted cross section more in line at higher energies with the results of Fuss *et al* [17], compared to those of Fuss *et al* [62].

3.3. Ionisation cross section

The neural network prediction for the ionisation cross section, plotted in figure 5, is agrees fairly well that of the de Urquijo *et al* [1] at low to intermediate energies, up to 100 eV, and thus also coincides well with the cross sections of Fuss *et al* [17], Swadia *et al* [34], Możejko and Sanche [29], and Bug *et al*

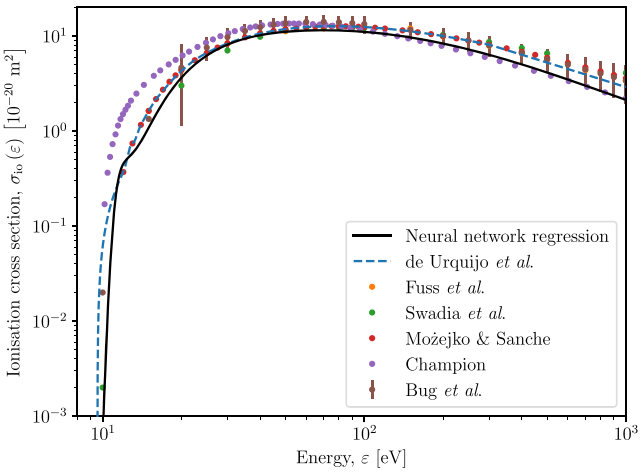

Figure 5. A comparison of the present neural network regression ionisation cross section, with a selection of earlier results [1, 13, 17, 29, 32, 34].

[13]. Beyond 100 eV, the machine-fitted cross section agrees particularly well with the theoretical result of Champion [32]. Although the neural network regression here suggested an ionisation threshold energy of 8.99 eV, it should be noted that increasing this threshold to 9.55 eV, the value adopted in references [1,37,39] from the experimental value of Dampc *et al* [31], did not result in any perceptible change to the simulated swarm transport coefficients.

3.4. Non-dissociative/dissociative electron attachment cross section

The measurement of electron attachment cross sections in THF has been concentrated mostly on DEA. The only experiment reporting the direct detection of a metastable negative ion $[THF]^{*-}$ is that of Sulzer *et al* [92], arising from a coordinated research between two laboratories at Innsbruck and Berlin, which differ only in the ion source. In the Innsbruck apparatus, the electron beam was produced by an electrostatic hemispherical electron monochromator while at Berlin the beam was generated from a trochoidal electron monochromator. Both ion sources had a similar energy resolution in the range 100–130 eV. Apart from these differences, in both devices the electron beam is made to intersect orthogonally with the effusive molecular beam. The ions are extracted by a small electric field toward the entrance of a quadrupole mass spectrometer and detected at its exit. A perfect agreement between the data obtained from both laboratories was reported.

Ibănescu *et al* [93] used a magnetically collimated trochoidal electron monochromator with a resolution of about 150 meV. The beam was focussed into the collision chamber filled with THF. The collision fragment anions were extracted and focussed into a quadrupole mass spectrometer. No THF^{-*} was detected, but it was recognised that the detection of these anions is very rare in DEA experiments well above non-thermal energies. Regarding the dissociation products, Ibănescu *et al* found that the most abundant ion was C_2HO^-, followed by H^- and $C_2H_2O^-$ over the combined energy range of 5–13 eV.

Using the Innsbruck apparatus, Sulzer *et al* [92] detected $C_4H_8O^-$ (THF^-), $C_4H_6O^-$ and C_2HO^-, with the negative ion yield of THF^- peaking at about 1 eV. Provided that this anion was observed at an energy above 1 eV, Sulzer *et al* concluded, without providing any further explanation, that the THF^- species detected was generated via secondary processes. In connection with this, if the ion is formed in the collision cell, the reaction rates leading to a secondary negative ion with a mass equal to that of THF would have to be very high.

Finally, Aflatooni *et al* [35] used a modified electron transmission spectrometer with a resolution similar to the above experiments and were able to measure an absolute DEA cross section in THF over the range 1–8.6 eV.

Even though Sulzer *et al* were the only group which detected THF^-, and provided that their energy resolution hindered them to explore lower energies close to thermal, we conclude that the existence of a THF^- species formed by resonant electron attachment cannot be ruled out at once. Furthermore, looking at the α_{eff} curves plotted in figure 8(b), the increasingly negative value of this swarm coefficient with decreasing E/n_0 (i.e. mean energy) strongly suggests the possibility of a resonantly formed THF^- species at energies well below 1 eV. In view of the need to extend the attachment cross section set down to energies so low as 10^{-4} eV in this research where only anions from the parent molecule may form, we shall refer to, regardless of the ion species, the present electron total attachment cross section as the non-dissociative/dissociative attachment (NDA–DEA) cross section.

The NDA–DEA cross section determined by the neural network is plotted in figure 6. Below 0.1 eV the present neural network prediction flattens, becoming constant in magnitude below 10^{-2} eV and differing significantly from the 'hand-fitted' NDA–DEA proposed by de Urquijo *et al* [1] which, by contrast, increases by over an order of magnitude down to 10^{-4} eV according to a rough power law. Although no explicit constraints were placed on the NDA–DEA fit—see figure 2(a) for the range of attachment training data used—the resulting neural network regression can be seen to agree fairly well overall within the experimental uncertainties of the measurements of both Aflatooni *et al* [35] and Janečková *et al* [36]. Beyond 16 eV, the neural network does not find any noticeable DEA, even though this possibility is by no means ruled out given the scope of examples used to train the network.

3.5. Grand TCS

As expected from the constraints placed on the training data, the cross sections determined by the neural network are consistent with the grand TCS of the de Urquijo *et al* [1] set. We show this in figure 7, by simply summing the entire cross section set with the quasi-elastic MTCS replaced by the quasi-elastic integral cross section derived by Casey *et al* [39] from the grand-TCS of Fuss *et al* [17]. Consequently, the resulting TCS also agrees fairly well with the experimental measurements of Baek *et al* [16], Bug *et al* [13], and Możejko *et al* [63] above 4 eV.

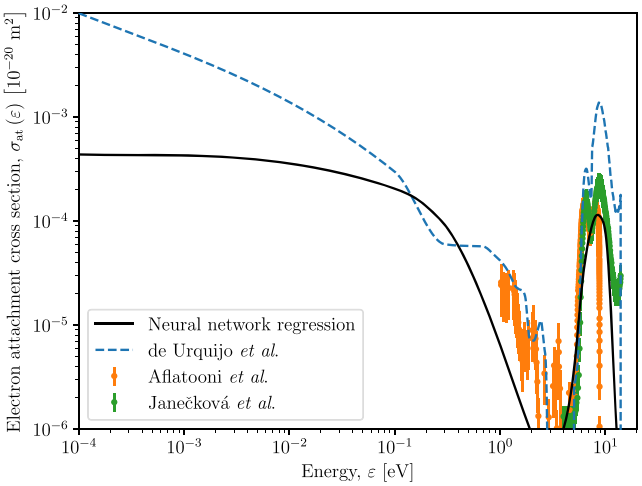

Figure 6. A comparison of the present neural network regression of the NDA–DEA cross section, alongside a selection of earlier results [1, 35, 36].

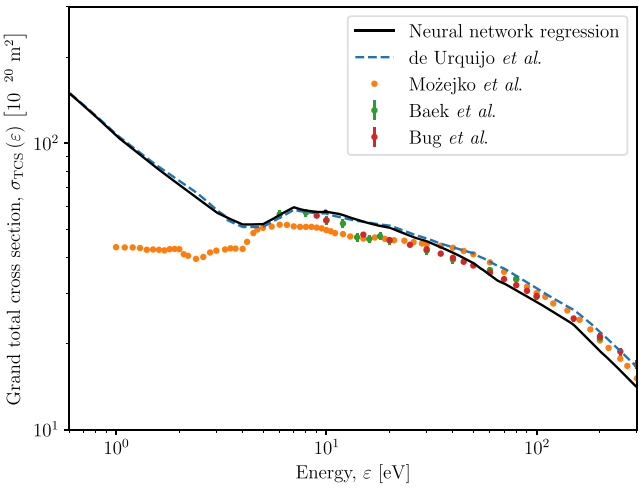

Figure 7. A comparison of the present neural network regression grand TCS, with a selection of earlier results [1, 13, 16, 63].

4. Transport coefficients for the refined cross section set

Transport coefficients are calculated using a two-term Boltzmann equation solver with the machine-fitted cross sections presented in the previous section, and are plotted in figure 8 for comparison against the measured pulsed-Townsend swarm data used to perform the fit, as well as corresponding transport coefficient values from the cross section data from de Urquijo *et al* [1]. Figure 8(a) plots the drift velocities, W, while figure 8(b) plots the effective Townsend first ionisation coefficients, α_{eff}/n_0. In addition, figures 8(c) and (d), respectively, plot their percentage differences relative to the experimental swarm data.

The neural network refined cross section set can be seen to improve the accuracy of the pure THF drift velocities, particularly at lower reduced fields where the error is now $< 5\%$. At higher fields, there is still an improvement with the difference

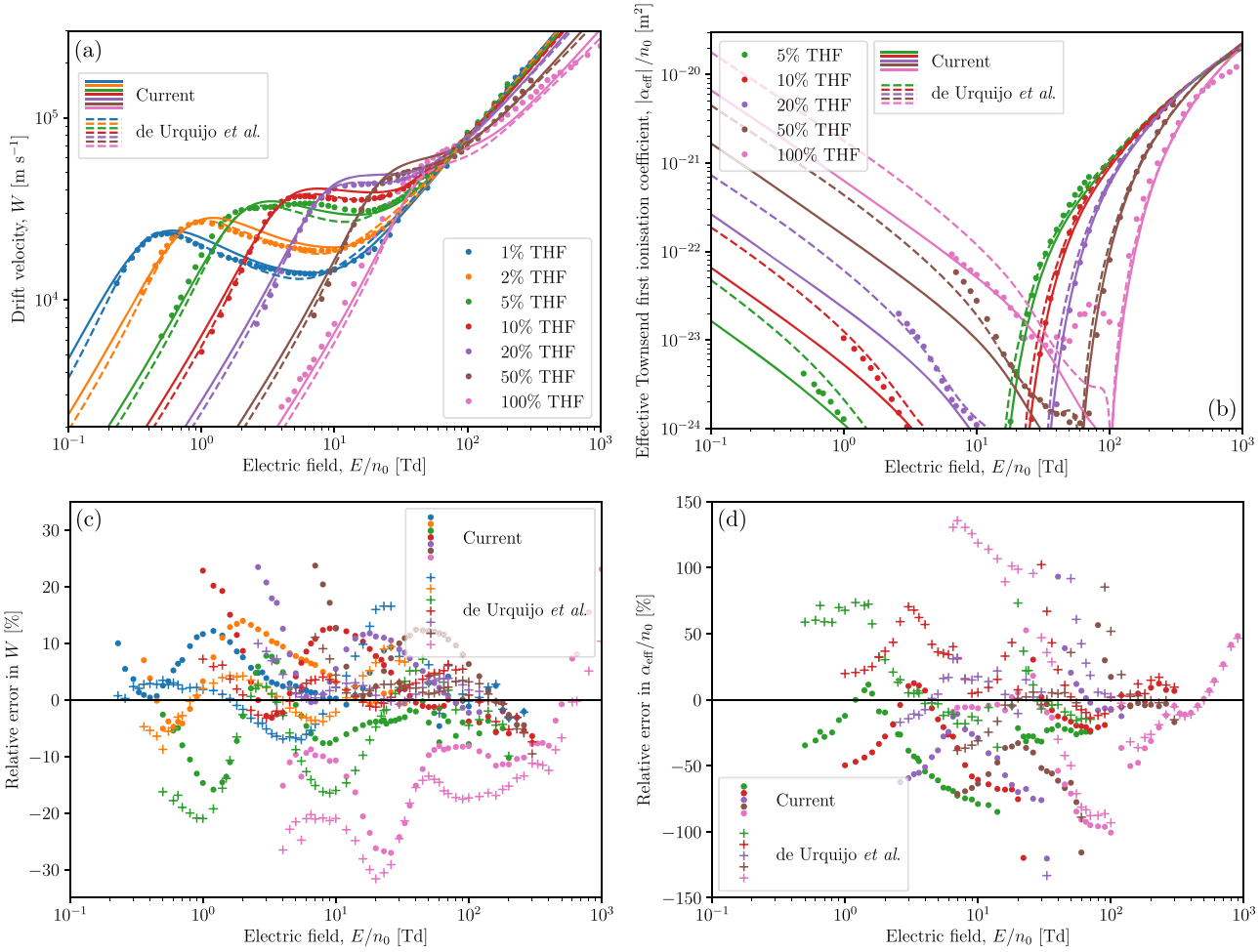

Figure 8. Simulated transport coefficients (solid curves) of, (a), flux drift velocity, W, and, (b), effective Townsend first ionisation coefficient, $\alpha_{\rm eff}/n_0$, for the neural network refined cross section set, alongside corresponding percentage error plots (c) and (d), respectively. Note that some outlying percentage error markers in (d) have been truncated.

now $< 20\%$, rather than the $< 32\%$ difference found using the cross section set of reference [1]. A similar improvement can be seen for the 5% THF mixture ratio, but the same cannot be said for the remaining THF mixture ratios which have somewhat worsened the agreement at lower fields, possibly as a trade-off for the increased accuracy in the 5% and pure THF cases. The 10%, 20% and 50% THF mixtures were the worst affected, with differences compared to the measured swarm data reaching as high as 43% at the lowest fields considered.

For the effective Townsend first ionisation coefficient, the modified cross section set is seen to be generally comparable to the de Urquijo *et al* set, at least in terms of relative error. The qualitative form of the resultant transport coefficients, in the electronegative region, are however, generally poorer for the modified set compared to that for the de Urquijo *et al* [1] set, with the exception of the case of pure THF. In the electropositive region, the modified set results in Townsend coefficients that generally underestimate the experimental measurements. That said, the discrepancy between the measured and calculated effective Townsend coefficients, in this region, has clearly improved for the 20% and 50% THF mixtures, although worsened for pure THF.

Overall, we can conclude that the neural network model has produced a plausible THF cross section set that is of comparable quality to the recent hand-refined set of de Urquijo *et al* [1], while importantly being free from the subjectivity inherent to conventional swarm analysis 'by-hand'. The utility of this machine learning approach can be seen in particular by the fits of the low-energy neutral dissociation cross section, plotted in figure 4(a), and the NDA–DEA cross section, plotted in figure 6. In both cases, the model succeeds in deriving a plausible cross section in its entirety from the swarm data.

5. Conclusion

We have presented a set of electron–THF cross sections that refines that constructed by de Urquijo *et al* [1] by modifying its quasielastic MTCS, neutral dissociation, ionisation and electron attachment cross sections. A unique aspect of this work is that these proposed modifications were performed automatically by a neural network model that was trained in order to solve the electron–THF inverse swarm problem for realistic sets of cross sections taken from the LXCat project [58–60]. The resulting set of THF cross sections was found to be self-consistent, in that it accurately reproduced many of

the swarm measurements that were used to perform the fit. It was thus concluded that the resulting machine-refined cross section set was of a comparable quality to the hand-refined set of de Urquijo *et al* [1], though it was noted that both sets have their own strengths and weaknesses. Taking the subjectivity out of forming recommended cross section data sets (i.e. the 'by-hand' approach adopted previously in reference [1]), for describing the behavior of electrons as they travel through a background gas under the influence of an applied external electric field, is an important development and while further work clearly needs to be undertaken on our current neural network approach this study represents a step forward in achieving that goal.

Of the modifications to the de Urquijo *et al* [1] set that were proposed by the neural network, the largest changes were made to the low-energy neutral dissociation cross section, plotted in figure 4(a), and the electron attachment cross section, plotted in figure 6. This was expected, as no explicit constraints were placed on these cross sections in figure 2, leaving the neural network with the task of determining both in their entirety using the swarm data alone. This task of simultaneously determining multiple unknown cross sections entirely from swarm data is a daunting prospect and the apparent success of the neural network in this case highlights the utility of this automated approach to swarm analysis.

One limitation of the specific machine learning approach taken here is that it provides only a single proposed THF cross section set when it is evident that multiple are plausible. We intend to address this non-uniqueness of the inverse swarm problem through the use of alternative neural network architectures that allow for the uncertainty in the predicted cross sections to be quantified. Examples of such alternatives include mixture density networks [94] and conditional generative models [95–99].

In the future, we plan to also apply machine-assisted swarm analysis towards determining cross sections for other important molecules of biological interest, including tetrahydrofurfuryl alcohol [12, 63, 100–105] and water [106]. It is promising to note that, due to the data-driven nature of machine learning, such machine-adjusted cross section sets can continue to be revisited as the LXCat databases continue to grow and be refined [58,59].

Acknowledgments

The authors gratefully acknowledge the financial support of the Australian Research Council through the Discovery Projects Scheme (Grant #DP180101655). JdeU thanks PAPIIT-UNAM, Project IN118520 for support. GG acknowledges support from the Spanish Ministerio de Ciencia, Innovación y Universidades-MICIU (Projects FIS2016-80440 and PID2019-104727RB-C21) and CSIC (Project LINKA 20085).

ORCID iDs

P W Stokes https://orcid.org/0000-0002-0956-5927
M J E Casey https://orcid.org/0000-0003-0193-211X
D G Cocks https://orcid.org/0000-0002-9943-7100
J de Urquijo https://orcid.org/0000-0003-3379-9843
G García https://orcid.org/0000-0003-4033-4518
M J Brunger https://orcid.org/0000-0002-7743-2990
R D White https://orcid.org/0000-0001-5353-7440

References

[1] de Urquijo J, Casey M J E, Serkovic-Loli L N, Cocks D G, Boyle G J, Jones D B, Brunger M J and White R D 2019 *J. Chem. Phys.* **151** 054309
[2] Kong M G, Kroesen G, Morfill G, Nosenko T, Shimizu T, van Dijk J and Zimmermann J L 2009 *New J. Phys.* **11** 115012
[3] Laroussi M 2009 *IEEE Trans. Plasma Sci.* **37** 714–25
[4] Montie T C, Kelly-Wintenberg K and Roth J R 2000 *IEEE Trans. Plasma Sci.* **28** 41–50
[5] Fridman G, Peddinghaus M, Balasubramanian M, Ayan H, Fridman A, Gutsol A and Brooks A 2006 *Plasma Chem. Plasma Process.* **26** 425–42
[6] Nastuta A V, Topala I, Grigoras C, Pohoata V and Popa G 2011 *J. Phys. D: Appl. Phys.* **44** 105204
[7] Miller V, Lin A and Fridman A 2016 *Plasma Chem. Plasma Process.* **36** 259–68
[8] Tanaka H, Brunger M J, Campbell L, Kato H, Hoshino M and Rau A R P 2016 *Rev. Mod. Phys.* **88** 025004
[9] Boudaïffa B, Cloutier P, Hunting D, Huels M A and Sanche L 2000 *Science* **287** 1658–60
[10] Sanche L 2005 *Eur. Phys. J.* D **35** 367–90
[11] Alizadeh E, Orlando T M and Sanche L 2015 *Annu. Rev. Phys. Chem.* **66** 379–98
[12] Brunger M J 2017 *Int. Rev. Phys. Chem.* **36** 333–76
[13] Bug M U, Yong Baek W, Rabus H, Villagrasa C, Meylan S and Rosenfeld A B 2017 *Radiat. Phys. Chem.* **130** 459–79
[14] Zecca A, Perazzolli C and Brunger M J 2005 *J. Phys. B: At. Mol. Opt. Phys.* **38** 2079–86
[15] Możejko P, Ptasińska-Denga E, Domaracka A and Szmytkowski C 2006 *Phys. Rev.* A **74** 012708
[16] Baek W Y, Bug M, Rabus H, Gargioni E and Grosswendt B 2012 *Phys. Rev.* A **86** 032702
[17] Fuss M C, Sanz A G, Blanco F, Limão-Vieira P, Brunger M J and García G 2014 *Eur. Phys. J.* D **68** 161
[18] Colyer C J, Vizcaino V, Sullivan J P, Brunger M J and Buckman S J 2007 *New J. Phys.* **9** 41
[19] Dampc M, Milosavljević A R, Linert I, Marinković B P and Zubek M 2007 *Phys. Rev.* A **75** 042710
[20] Allan M 2007 *J. Phys. B: At. Mol. Opt. Phys.* **40** 3531–44
[21] Homem M G P, Sugohara R T, Sanches I P, Lee M T and Iga I 2009 *Phys. Rev.* A **80** 032705
[22] Gauf A, Hargreaves L R, Jo A, Tanner J, Khakoo M A, Walls T, Winstead C and McKoy V 2012 *Phys. Rev.* A **85** 052717
[23] Zhang L, Sun W, Zhang Y, Fan Z, Hu S and Fan Q 2017 *J. Phys. B: At. Mol. Opt. Phys.* **50** 085201
[24] Dampc M, Linert I, Milosavljević A R and Zubek M 2007 *Chem. Phys. Lett.* **443** 17–21
[25] Khakoo M A, Orton D, Hargreaves L R and Meyer N 2013 *Phys. Rev.* A **88** 012705
[26] Duque H V, Do T P T, Lopes M C A, Konovalov D A, White R D, Brunger M J and Jones D B 2015 *J. Chem. Phys.* **142** 124307
[27] Do T P T, Leung M, Fuss M, Garcia G, Blanco F, Ratnavelu K and Brunger M J 2011 *J. Chem. Phys.* **134** 144302
[28] Zubek M, Dampc M, Linert I and Neumann T 2011 *J. Chem. Phys.* **135** 134317
[29] Możejko P and Sanche L 2005 *Radiat. Phys. Chem.* **73** 77–84

[30] Fuss M, Muñoz A, Oller J C, Blanco F, Almeida D, Limão-Vieira P, Do T P D, Brunger M J and García G 2009 *Phys. Rev.* A **80** 052709
[31] Dampc M, Szymańska E, Mielewska B and Zubek M 2011 *J. Phys. B: At. Mol. Opt. Phys.* **44** 055206
[32] Champion C 2013 *J. Chem. Phys.* **138** 184306
[33] Builth-Williams J D *et al* 2013 *J. Chem. Phys.* **139** 034306
[34] Swadia M, Thakar Y, Vinodkumar M and Limbachiya C 2017 *Eur. Phys. J.* D **71** 85
[35] Aflatooni K, Scheer A M and Burrow P D 2006 *J. Chem. Phys.* **125** 054301
[36] Janečková R, May O, Milosavljević A and Fedor J 2014 *Int. J. Mass Spectrom.* **365-366** 163–8
[37] Garland N A, Brunger M J, Garcia G, de Urquijo J and White R D 2013 *Phys. Rev.* A **88** 062712
[38] Swadia M, Bhavsar R, Thakar Y, Vinodkumar M and Limbachiya C 2017 *Mol. Phys.* **115** 2521–7
[39] Casey M J E, de Urquijo J, Serkovic Loli L N, Cocks D G, Boyle G J, Jones D B, Brunger M J and White R D 2017 *J. Chem. Phys.* **147** 195103
[40] White R D *et al* 2018 *Plasma Sources Sci. Technol.* **27** 053001
[41] Mayer H F 1921 *Ann. Phys.* **369** 451–80
[42] Ramsauer C 1921 *Ann. Phys.* **369** 513–40
[43] Townsend J S and Bailey V A 1922 *London Edinburgh Dublin Philos. Mag. J. Sci.* **43** 593–600
[44] Frost L S and Phelps A V 1962 *Phys. Rev.* **127** 1621–33
[45] Engelhardt A G and Phelps A V 1963 *Phys. Rev.* **131** 2115–28
[46] Engelhardt A G, Phelps A V and Risk C G 1964 *Phys. Rev.* **135** A1566–74
[47] Hake R D and Phelps A V 1967 *Phys. Rev.* **158** 70–84
[48] Phelps A V 1968 *Rev. Mod. Phys.* **40** 399–410
[49] Duncan C W and Walker I C 1972 *J. Chem. Soc. Faraday Trans. II* **68** 1514
[50] O'Malley T F and Crompton R W 1980 *J. Phys. B: At. Mol. Phys.* **13** 3451–64
[51] Taniguchi T, Suzuki M, Kawamura K, Noto F and Tagashira H 1987 *J. Phys. D: Appl. Phys.* **20** 1085–7
[52] Suzuki M, Taniguchi T and Tagashira H 1989 *J. Phys. D: Appl. Phys.* **22** 1848–55
[53] Suzuki M, Taniguchi T and Tagashira H 1990 *J. Phys. D: Appl. Phys.* **23** 842–50
[54] Morgan W L 1991 *Phys. Rev.* A **44** 1677–81
[55] Morgan W L 1993 *J. Phys. D: Appl. Phys.* **26** 209–14
[56] Brennan M and Ness K 1993 *Aust. J. Phys.* **46** 249
[57] Stokes P W, Cocks D G, Brunger M J and White R D 2020 *Plasma Sources Sci. Technol.* **29** 055009
[58] Pancheshnyi S, Biagi S, Bordage M C, Hagelaar G J M, Morgan W L, Phelps A V and Pitchford L C 2012 *Chem. Phys.* **398** 148–53
[59] Pitchford L C *et al* 2017 *Plasma Process. Polym.* **14** 1600098
[60] LXCat www.lxcat.net
[61] Ramachandran P, Zoph B and Le Q V 2017 arXiv:1710.05941
[62] Fuss M C *et al* 2012 *J. Phys.: Conf. Ser.* **373** 012010
[63] Możejko P, Domaracka A, Ptasińska-Denga E and Szmytkowski C 2006 *Chem. Phys. Lett.* **429** 378–81
[64] Biagi database www.lxcat.net/Biagi
[65] Biagi-v7.1 database www.lxcat.net/Biagi-v7.1
[66] Bordage database www.lxcat.net/Bordage
[67] BSR database www.lxcat.net/BSR
[68] CCC database www.lxcat.net/CCC
[69] Christophorou database www.lxcat.net/Christophorou
[70] COP database www.lxcat.net/COP
[71] eMol-LeHavre database www.lxcat.net/eMol-LeHavre
[72] FLINDERS database www.lxcat.net/FLINDERS
[73] Hayashi database www.lxcat.net/Hayashi
[74] IST-Lisbon database www.lxcat.net/IST-Lisbon
[75] Itikawa database www.lxcat.net/Itikawa
[76] Morgan database www.lxcat.net/Morgan
[77] NGFSRDW database www.lxcat.net/NGFSRDW
[78] Phelps database www.lxcat.net/Phelps
[79] QUANTEMOL database www.lxcat.net/QUANTEMOL
[80] SIGLO database www.lxcat.net/SIGLO
[81] TRINITI database www.lxcat.net/TRINITI
[82] Hagelaar G J M and Pitchford L C 2005 *Plasma Sources Sci. Technol.* **14** 722–33
[83] Robson R E and Ness K F 1986 *Phys. Rev.* A **33** 2068–77
[84] Sherman B 1960 *J. Math. Anal. Appl.* **1** 342–54
[85] Hairer E, Nørsett S P and Wanner G 1993 *Solving Ordinary Differential Equations I* (*Springer Series in Computational Mathematics* vol 8) (Berlin: Springer)
[86] Rackauckas C and Nie Q 2017 *J. Open Res. Softw.* **5** 15
[87] DelayDiffEq.jl github.com/JuliaDiffEq/DelayDiffEq.jl
[88] OrdinaryDiffEq.jl github.com/JuliaDiffEq/OrdinaryDiffEq.jl
[89] Innes M 2018 *J. Open Source Softw.* **3** 602
[90] Glorot X and Bengio Y 2010 Understanding the difficulty of training deep feedforward neural networks *Proc. of the 13th Int. Conf. on Artificial Intelligence and Statistics* vol 9 ed Y W Teh and M Titterington (Chia Laguna Resort, Sardinia, Italy) (Proceedings of Machine Learning Research) pp 249–56
[91] Kingma D P and Ba J L 2015 Adam: a method for stochastic optimization *3rd Int. Conf. on Learning Representations*
[92] Sulzer P *et al* 2006 *J. Chem. Phys.* **125** 044304
[93] Ibănescu B C, May O and Allan M 2008 *Phys. Chem. Chem. Phys.* **10** 1507
[94] Bishop C M 1994 Mixture density networks http://publications.aston.ac.uk/id/eprint/373/
[95] Sohn K, Lee H and Yan X 2015 Learning structured output representation using deep conditional generative models *Advances in Neural Information Processing Systems* vol 28 ed C Cortes, N D Lawrence, D D Lee, M Sugiyama and R Garnett (Curran Associates, Inc.) pp 3483–91
[96] Mirza M and Osindero S 2014 arXiv:1411.1784
[97] Dinh L, Krueger D and Bengio Y 2015 *3rd Int. Conf. on Learning Representations, ICLR 2015—Workshop Track Proc.*
[98] Dinh L, Sohl-Dickstein J and Bengio S 2016 arXiv:1605.08803
[99] Kingma D P and Dhariwal P 2018 Glow: generative flow with invertible 1x1 convolutions *Advances in Neural Information Processing Systems 31* ed S Bengio, H Wallach, H Larochelle, K Grauman, N Cesa-Bianchi and R Garnett (Curran Associates, Inc.) pp 10215–24
[100] Jones D B *et al* 2013 *Chem. Phys. Lett.* **572** 32–7
[101] Limão-Vieira P, Duflot D, Hubin-Franskin M-J, Delwiche J, Hoffmann S V, Chiari L, Jones D B, Brunger M J and Lopes M C A 2014 *J. Phys. Chem.* A **118** 6425–34
[102] Duque H V *et al* 2014 *Chem. Phys. Lett.* **608** 161–6
[103] Bellm S M *et al* 2012 *J. Chem. Phys.* **136** 244301
[104] Duque H V *et al* 2014 *J. Chem. Phys.* **140** 214306
[105] Chiari L *et al* 2014 *J. Chem. Phys.* **141** 024301
[106] White R D, Brunger M J, Garland N A, Robson R E, Ness K F, Garcia G, de Urquijo J, Dujko S and Petrović Z L 2014 *Eur. Phys. J.* D **68** 125